# Self-phase-locked divide-by-2 optical parametric oscillator as a broadband frequency comb source

**Samuel T. Wong,[1,2] Konstantin L. Vodopyanov,[1,*] and Robert L. Byer[1]**

[1]*E. L. Ginzton Laboratory, Stanford University, Stanford, California 94305, USA*
[2]*Q-Peak, Inc., 135 South Road, Bedford, Massachusetts 01730, USA*
[*]*Corresponding author: vodopyan@stanford.edu*

Received January 4, 2010; revised February 25, 2010; accepted February 25, 2010;
posted February 25, 2010 (Doc. ID 122157); published April 6, 2010

We investigate, both theoretically and experimentally, spectral, temporal, and coherence properties of a degenerate synchronously pumped optical parametric oscillator (SPOPO) as a divide-by-2 subharmonic generator. Periodically poled lithium niobate was used as the nonlinear gain medium and 180 fs pulses from a mode-locked Ti:Sapphire laser as the pump. A regime of stable SPOPO operation at degeneracy was achieved, where the SPOPO longitudinal modes were phase-locked to the pump, even without active cavity-length stabilization. Phase locking was confirmed by interference measurements between the pump and the frequency-doubled optical parametric oscillator output, as well as by beat frequency measurements using an independent continuous-wave laser. We have found that the stability range of such a phase-locked state, with respect to external perturbations, increased with the pump power and decreased with the cavity $Q$ at a constant number of times above threshold, in excellent agreement with our model based on coupled nonlinear wave equations. At degeneracy (around 1550 nm), the SPOPO produced 70 fs output pulses with the full width at half-maximum spectral width of 210 $cm^{-1}$, which manifests significant pulse compression and spectral broadening with respect to the pump laser. 

*OCIS codes:* 190.4970, 190.7110.

## 1. INTRODUCTION

Broadband optical frequency comb sources based on simultaneously mode-locked and carrier-envelope-phase-stabilized femtosecond lasers in the ultraviolet, visible, and near-infrared (IR) wavelength ranges have become ubiquitous in time and frequency metrology [1,2]. The most recent applications of frequency combs include astronomical observations [3], ultrasensitive molecular spectroscopy based on both parallel spectral detection [4], and coherent multi-heterodyne Fourier transform spectroscopy [5–7].

Extending the range of phase-stabilized few-optical-cycle pulses to longer wavelengths is critical for such applications as molecular spectroscopy and trace gas detection, since one can reach the most desirable range of frequency combs corresponding to fundamental rotational-vibrational resonances; for high harmonic generation in gases, because at longer wavelengths one can achieve longer acceleration cycle for an electron escaping the atom [8,9]; and for vacuum-based laser-driven particle acceleration [10,11] using photonic crystal structures [12], since with longer wavelengths one can avoid two-photon absorption in the latter.

Several methods were developed recently for extending ultrafast frequency comb sources to longer wavelengths. These include direct laser sources in the mid-IR [6,13], supercontinuum generation via spectral broadening in optical fibers [14–16] and engineered $\chi^{(2)}$ nonlinear optical devices [17], optical rectification [18,19], difference-frequency generation schemes [20–23], and optical parametric oscillators (OPOs) [24,25] and amplifiers [26].

OPOs are ideal candidates for extending frequency combs to the IR via optical frequency division. The implementation of OPOs as divide-by-$N$ subharmonic generators allows downconverting pump photons into highly phase-correlated signal and idler photons. Phase-locked frequency division by 2 was observed in a type I phase-matched continuous-wave (CW) OPO [27], whose co-polarized signal and idler become truly degenerate when their frequencies are equal. Experimental and theoretical studies were also done for type II phase-matched CW OPOs where an intracavity quarter-wave plate was used to induce coupling between orthogonal polarizations of the signal and idler for injection locking to occur [28–33]. Extensive research has been carried out on divide-by-3 OPOs where the photon energy ratio for the pump, signal, and idler is 3:2:1, respectively [34–36]. The phase relation among the pump, signal, and idler pulses of a divide-by-3 femtosecond OPO pumped by a Ti:Sapphire laser was measured [37] and phase locking was achieved [38,39] using active electronic control of cavity lengths.

This work presents what we believe to be a new approach to creating IR frequency combs by using a type 0 phase-matched divide-by-2 OPO pumped by a femtosecond laser (type 0 OPO is a type I OPO with the pump, signal, and idler polarizations parallel). It extends the results of our previous work on the first demonstration of a self-phase-locked subharmonic OPO [40,41]. One advantage for choosing this configuration is the potential for high (>90%) conversion efficiency where most of the pump photons are converted into signal/idler pairs. Also, type 0 phase-matching is characterized by an extremely wide bandwidth near degeneracy and, in the case of lithium niobate, exploits the highest available nonlinear

 

coefficient ($d_{33}$). Another advantage is that passive optical phase locking can be achieved even without active electronic stabilization.

The paper is organized in the following way. First, we consider oscillation conditions for a degenerate synchronously pumped optical parametric oscillator (SPOPO), develop a simple theory based on coupled nonlinear optical wave equations, for self-phase-locking of the OPO modes to those of the pump, and explore the stability conditions of the phase-locked state. Next, we compare our predictions with experimental data and make final conclusions.

## 2. LOCKING CONDITIONS FOR THE DEGENERATE SPOPO

In an OPO, the photon energy conservation dictates that

$$\nu_p = \nu_s + \nu_i, \tag{1}$$

and, also, there is a fixed phase relationship between the pump, signal, and idler waves,

$$\phi_p = \phi_s + \phi_i + \pi/2, \tag{2}$$

so that the energy flow is from the pump to the signal and the idler pair [42]. Here $\nu_p$, $\nu_s$, and $\nu_i$ are the pump, signal, and idler frequencies, and $E_p = E_p \cos(2\pi\nu_p t + \phi_p)$, $E_s = E_s \cos(2\pi\nu_s t + \phi_s)$, and $E_i = E_i \cos(2\pi\nu_i t + \phi_i)$ are the electric fields ($E$-fields) of the pump, signal, and idler, correspondingly. For a non-degenerate OPO, the signal and idler phases, $\phi_s$ and $\phi_i$, are free to adopt any value as long as Eq. (2) is satisfied. This degree of freedom disappears when the (co-polarized) signal and idler become indistinguishable at degeneracy, which leads to $\phi_s = \phi_i$. Hence, Eq. (2) becomes

$$\phi_p = 2\phi_{s,i} + \pi/2, \tag{3}$$

and the phase coherence between the OPO and the pump is established. Note that when the signal and idler $E$-fields simultaneously change their phases by $\pi$ (flip sign), the total phase difference changes by $2\pi$, such that Eq. (3) still remains valid [27].

The locking analysis for the degenerate SPOPO is a little more complicated than that for the CW OPO with a monochromatic pump due to the multi-axial-mode structure of the SPOPO. However, the main features remain the same. The pump field is represented by a frequency comb,

$$\nu_n = f_{\mathrm{CEO}} + n f_{\mathrm{rep}}, \tag{4}$$

with mode separation $f_{\mathrm{rep}}$ (Fig. 1) corresponding to the pulse repetition rate, $n$ as the mode number (centered at some large $n_0 = 10^6 - 10^7$), and $f_{\mathrm{CEO}}$ as the carrier-envelope offset (CEO) frequency ($0 \le f_{\mathrm{CEO}} < f_{\mathrm{rep}}$). For the degenerate SPOPO [Fig. 1(c)], such that the signal and the idler overlap near half of the pump center frequency, the OPO frequency comb is expressed as

$$\nu_m = \frac{f_{\mathrm{CEO}}}{2} + m f_{\mathrm{rep}}, \tag{5}$$

or

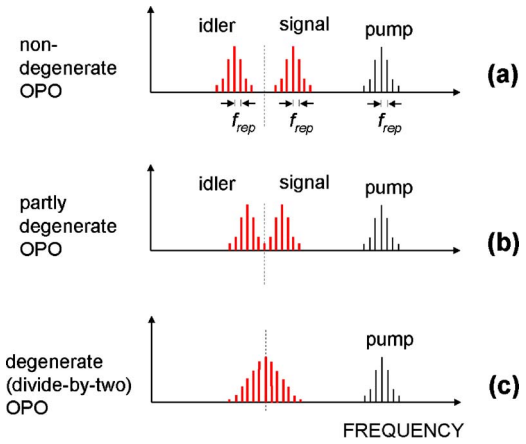


Fig. 1. (Color online) Longitudinal modes of (a) non-degenerate, (b) partly degenerate, and (c) degenerate SPOPO. Dashed line corresponds to the half of the pump center frequency.

$$\nu_m = \frac{f_{\mathrm{CEO}}}{2} + \left(m + \frac{1}{2}\right) f_{\mathrm{rep}}, \tag{6}$$

where $m$ is the OPO mode number (centered around some $m_0$ which is the closest integer to $n_0/2$). Figure 2 illustrates positions of longitudinal modes of a degenerate SPOPO with respect to those of the pump. Relations (5) and (6) result (i) from the photon energy conservation if one regards, as an elementary act, a decay of a particular pump mode into a signal plus idler modes and (ii) from the fact that the frequency spacing between neighboring OPO longitudinal modes has to be the same as for the pump (per SPOPO condition). The distinction between Eqs. (5) and (6) comes from the fact that the OPO frequency grid $\nu_m$ can either correspond to one half of the frequencies of the even modes (4) of the pump laser $\nu_{2p}$ or odd modes $\nu_{2p+1}$, where $p$ is an integer.

For a mode-locked pump laser, all its modes are—by definition—in phase. For simplicity, these phases can be set to zero by an appropriate choice of time origin: $\phi_n = 0$. In a non-degenerate OPO, constant phase relations will be established separately among the signal and idler modes. Suppose that a pump mode number $n$ (Fig. 3) decays into the idler mode number $m$ and signal mode num-

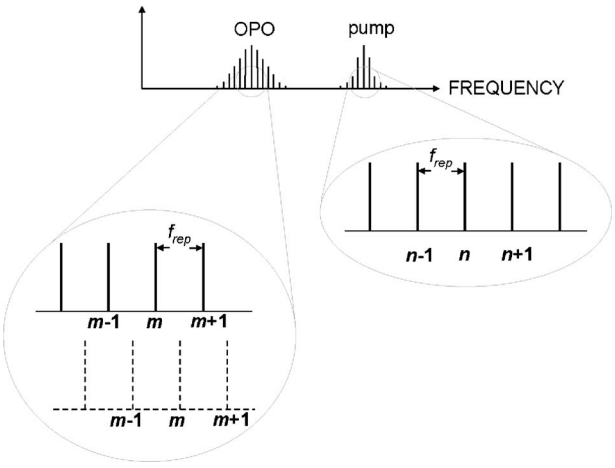


Fig. 2. Longitudinal modes of the pump and a degenerate doubly resonant SPOPO, which has two possible sets of modes.

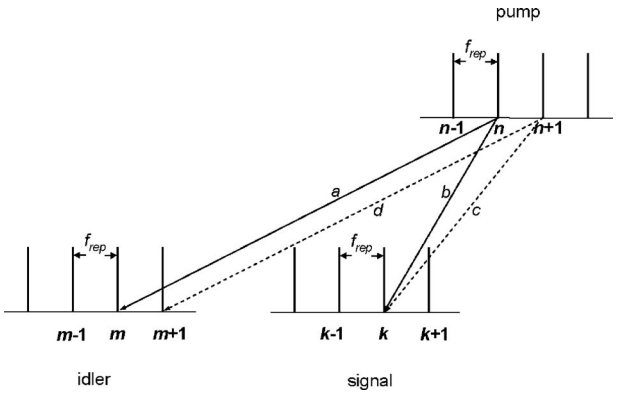


Fig. 3. Phase coherence between neighboring OPO modes is established via cross-coupling between the pump, signal, and idler, e.g., via *abcd* path.

ber $k$. If the phase of the $m$th idler mode is $\phi_m$, from Eq. (2) it follows that the phase of the signal mode $k$ has to be $\phi_k = -\pi/2 - \phi_m$. Now, if a laser mode number $n+1$ decays into the idler mode $m+1$ and signal mode $k$, the phase of the $(m+1)$th idler mode has to be $\phi_{m+1} = -\pi/2 - \phi_k = -\pi/2 - (-\pi/2 - \phi_m) = \phi_m$. This mechanism locks the phases (via *abcd* path in Fig. 3) of neighboring idler modes and thus locks all idler modes. The same is true for the signal. In a *degenerate* OPO, the signal and the idler overlap. Because of the cross-coupling, a constant phase is established through the common set of signal-plus-idler modes, which become phase-locked to those of the pump, and relation (3) becomes

$$\phi_n = 2\phi_m + \pi/2. \tag{7}$$

Here the index $m$ refers to the common signal-plus-idler set of OPO modes. Since $\phi_n$ is a constant, $\phi_m$ is also a constant and SPOPO modes become phase-coherent with those of the pump laser. In particular, when $\phi_n = 0$, $\phi_m = -\pi/4$, or $\phi_m = -\pi/4 + \pi = 3\pi/4$.

## 3. THEORETICAL MODEL FOR THE FREQUENCY LOCKING RANGE

In a doubly resonant OPO, both the signal and the idler frequencies must coincide with the longitudinal modes (resonances) of the OPO cavity, which is achieved by fine tuning of the cavity length on a subwavelength scale. Because of external perturbations, the OPO resonances fluctuate in frequency by some value $\Delta f$, with respect to the grid of OPO frequencies (5) and (6) determined by the frequency grid of the pump laser (Fig. 4). This mismatch causes an additional round trip phase $\varphi = 2\pi \times \Delta f / f_{\mathrm{rep}}$ (for *both* the signal and the idler).

For zero wave-vector mismatch, plane-wave approximation, and absence of pump depletion, the propagation of the normalized signal and idler $E$-fields, $A_s = (n_s/\omega_s)^{1/2} E_s$ and $A_i = (n_i/\omega_i)^{1/2} E_i$, through the nonlinear crystal can be written in the matrix form [43],

$$\begin{bmatrix} A_s(z=l) \\ A_i^*(z=l) \end{bmatrix} = \begin{vmatrix} \cosh(gl) & i\sinh(gl) \\ -i\sinh(gl) & \cosh(gl) \end{vmatrix} \begin{bmatrix} A_s(z=0) \\ A_i^*(z=0) \end{bmatrix}. \tag{8}$$

The asterisk denotes complex conjugate, $n_{s,i}$ and $\omega_{s,i}$ are the signal and idler refractive indices and angular frequencies correspondingly, $l$ is the nonlinear crystal length, and $g$ is the gain coefficient, which is proportional to the nonlinear optical coefficient $d_{\mathrm{eff}}$ and to the pump field $E_p$.

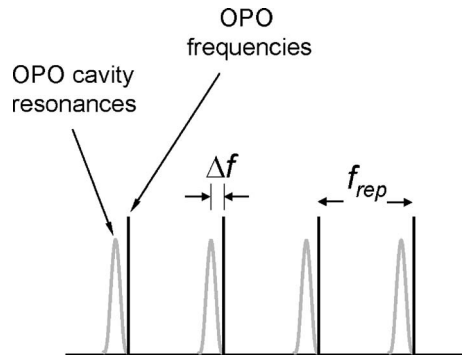


Fig. 4. SPOPO cavity resonances and SPOPO frequencies in the degenerate phase-locked regime.

Taking into account the intracavity loss, which is expressed through the roundtrip $E$-field transmission $t$ (such that the fractional power loss per round trip is $\mathrm{loss} = 1 - t^2$), and a round trip extra phase shift $\varphi$, due to the cavity-length mismatch, we can write the cavity round trip transfer matrix as

$$\mathbf{M} = \begin{vmatrix} t & 0 \\ 0 & t \end{vmatrix} \begin{vmatrix} e^{i\varphi} & 0 \\ 0 & e^{-i\varphi} \end{vmatrix} \begin{vmatrix} \cosh(gl) & i\sinh(gl) \\ -i\sinh(gl) & \cosh(gl) \end{vmatrix} = \begin{vmatrix} te^{i\varphi}\cosh(gl) & ite^{i\varphi}\sinh(gl) \\ -ite^{-i\varphi}\sinh(gl) & te^{-i\varphi}\cosh(gl) \end{vmatrix}. \tag{9}$$

From self-consistency, the following condition should be met:

$$\mathbf{A} = \mathbf{MA}, \tag{10}$$

and for a nontrivial solution, we get

$$\det|\mathbf{M} - \mathbf{I}| = 0, \tag{11}$$

where $\mathbf{I}$ is the unit matrix. From this we derive the following relation:

$$t^2 - 2t\cosh(gl)\cos\varphi + 1 = 0. \tag{12}$$

For the small loss in the cavity and for the small $\varphi$, we can approximate $\cosh(gl) \approx 1 + (gl)^2/2$ and $\cos(\varphi) \approx 1 - \varphi^2/2$. Taking into account that $\mathrm{loss} = 1 - t^2$, we obtain

$$(gl)^2 = (\mathrm{loss}/2)^2 + \varphi^2. \tag{13}$$

Since the condition of the doubly resonant OPO threshold is $(gl)_0^2 = (\mathrm{loss}/2)^2$ [43], we obtain the main result for the maximum allowed extra phase,

$$\varphi = (gl)_0\sqrt{N-1} = \frac{\mathrm{loss}}{2}\sqrt{N-1}. \tag{14}$$

Here we took into account that $(gl)^2$ is proportional to the pump power and $N = (gl)^2/(gl)_0^2$—the number of times above the oscillation threshold for the pump power. Finally we get

$$\frac{\Delta f}{f_{\text{rep}}} = \frac{\varphi}{2\pi} = \frac{\text{loss}}{4\pi}\sqrt{N-1}. \quad (15)$$

We note here that the self-phase-locked stability range $\Delta f$ increases with the pump power, and decreases with the cavity $Q$, at a fixed number of times above threshold.

## 4. EXPERIMENTAL CHARACTERIZATION OF THE DEGENERATE SPOPO

The SPOPO consisted of a near-symmetrically folded linear confocal cavity [40] as shown in Fig. 5. A Ti:Sapphire mode-locked laser (180 fs pulses at 80 MHz) with the center wavelength of 775 nm was used as a pump. The nonlinear gain element was an antireflection-coated (at 775 and 1550 nm) 1 mm long periodically poled magnesium oxide-doped lithium niobate (PPMgO:LN) crystal (HC Photonics, Inc.) with the poling period of 18.92 $\mu$m, kept at $t=140\,^{\circ}\text{C}$, and designed for type 0 (e-ee) phase-matched 1550 nm subharmonic generation. A 6 mm thick fused silica plate was placed inside the cavity to compensate the second-order dispersion of lithium niobate. The transition between degenerate and non-degenerate SPOPO operations was performed by changing the cavity length—the amount of detuning required to switch between these two states was about 5 $\mu$m. Figure 6 compares the two spectra—for degenerate and non-degenerate SPOPO operations—obtained with an optical spectrum analyzer. The 3 dB spectral bandwidth of the combined signal and idler at degenerate operation around 1550 nm was 50 nm (210 $\text{cm}^{-1}$). Taking into account that the pump laser bandwidth was 75 $\text{cm}^{-1}$, the degenerate SPOPO exhibited an output comb broadening by a factor of 2.6. The fringes in the degenerate SPOPO spectrum are related to the etalon effects from a glass slide used to outcouple some optical power to measure the spectrum. These ripples consistently appear across all the measured spectra in this particular setup and they can be regarded as an experimental artifact.

Figure 7 compares autocorrelation traces for degenerate and non-degenerate SPOPOs. The full width at half-maximum pulse duration in the degenerate case was 70 fs, which is close to transform-limited for the measured spectral width and a Gaussian profile. In contrast, the pulse shape for the non-degenerate SPOPO was broader and distorted. In fact, when the OPO is not degenerate, there can be arbitrary (and fluctuating) phase relations between the signal and the idler. Since the output pulse is formed by both signal and idler waves, that may cause the observed time-domain distortions.

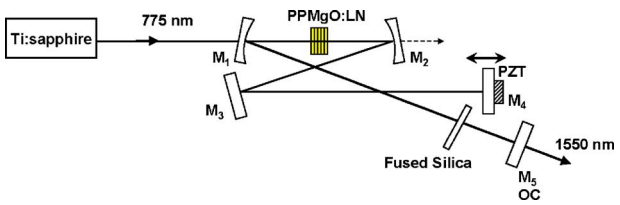


Fig. 5. (Color online) Schematic diagram of the degenerate type 0 SPOPO. Mirrors $M_1$–$M_4$ are highly reflective at 1550 nm, and $M_5$ is an OC mirror.

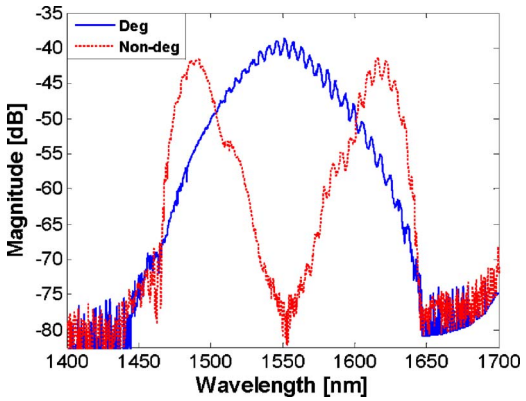


Fig. 6. (Color online) Spectra of the non-degenerate (dotted line) and degenerate (solid line) SPOPOs.

To measure the phase coherence between the pump and the OPO modes, the second harmonic (SH) of the SPOPO output (produced in a separate PPMgO:LN crystal) was compared with the pump, through small-angle interference patterns and through a radio frequency (RF) beat signal. If the SPOPO is phase-locked, interference between the pump and the frequency-doubled OPO output should yield a stable fringe pattern [note that both solutions (5) and (6) will produce the same SH field]. In addition, when the SPOPO is phase locked, Eqs. (5) and (6) require that the RF spectrum should exhibit only harmonics of $f_{\text{rep}}$ with no satellite beat notes. Because the SH crystal also produces, due to intermodal cross mixing, sum frequency generation (SFG) that fully reconstructs the pump, we examined narrow portions of the OPO SH spectrum to avoid most of the SFG background. Various narrowband (typically 3–10 nm wide) filters were placed: (i) after the SH crystal (thus filtering out the OPO SH spectrum) or (ii) before the SH crystal (thus filtering out the fundamental OPO spectrum), and delivered identical results for both fringe pattern and RF spectrum (Figs. 8 and 9). When the SPOPO was degenerate, a stable fringe pattern persisted with high contrast and no satellite RF beat notes were observed. In contrast, when the SPOPO was non-degenerate, stable fringes disappeared, while RF satellite beat notes emerged.

As another technique to confirm phase locking, we used an independent laser source—a single-mode 1550 nm CW

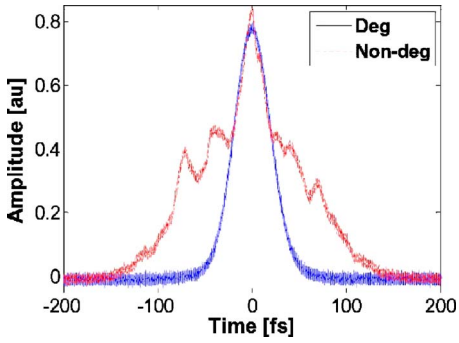


Fig. 7. (Color online) Background-free autocorrelation traces obtained using SH generation. Degenerate phase-locked SPOPO pulses (solid line) are transformed-limited with pulse duration of 70 fs. The pulse profile is distorted for non-degenerate (unlocked) SPOPO output (dashed line).

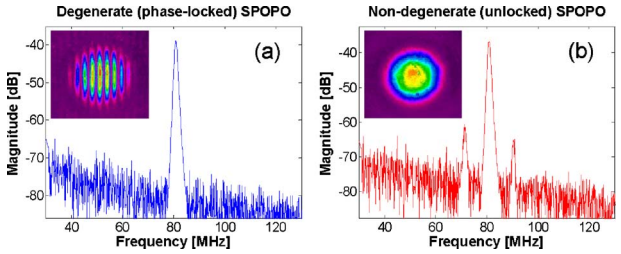


Fig. 8. (Color online) Results from interference measurements between the pump and the OPO SH transmitted through a narrowband 750 nm filter. (a) Degenerate (phase-locked) SPOPO. Presence of strongly visible fringes and absence of satellite RF beat frequencies can be seen; (b) non-degenerate (unlocked) SPOPO. There is an absence of fringe pattern and a presence of RF satellite beat notes.

laser and its SH—as an external phase reference to separately generate beat notes with the pump mode-locked laser and the SPOPO. The CEO frequency of the pump laser $f_{CEO}$ (4) was allowed to fluctuate to observe how the SPOPO would react to an evolving frequency offset of the pump frequency comb. If the SPOPO is degenerate and phase-locked to the pump, the change in the beat note between the SPOPO and the CW laser should be half of the change in the beat note between the pump and the frequency-doubled CW laser. In fact, the frequency of the CW laser can be represented as $\nu_0+kf_{rep}$, where $k$ is some large integer, and the beat note between its SH and the pump laser is $2\nu_0-f_{CEO}$. On the other hand, according to Eqs. (5) and (6) the beat note between the CW laser and the OPO is either $\nu_0-f_{CEO}/2$ or $\nu_0-f_{CEO}/2+f_{rep}/2$ (plus an integer number of $f_{rep}$). Figure 10 shows the scatter plot of the SPOPO beat frequency (within the 80 MHz window) versus the pump beat frequency drift. The SPOPO beat notes may jump randomly by 40 MHz ($f_{rep}/2$), after blocking and unblocking the pump beam, which corresponds to the two sets of SPOPO modes, both giving the slope of 1/2 as expected. This proves that the degenerate SPOPO automatically tracked $f_{CEO}$ of the drifting pump laser. Thus, for a CEO-stabilized pump, the SPOPO output will also be CEO-stabilized and phase-locked to the pump.

We measured the effect of cavity-length detuning for the SPOPO in the phase-locked state by dithering a highly reflective end mirror with a piezoelectric transducer (Fig. 5) while detecting the SPOPO output using a photodetector. The maximum length detuning $\Delta L$, before the oscillation ceases, is related to the frequency locking range $\Delta f$ via the relation $\Delta f/f_{rep}=\Delta L/(\lambda/2)$, where $\lambda=1550$ nm is the central SPOPO wavelength. Figure 11

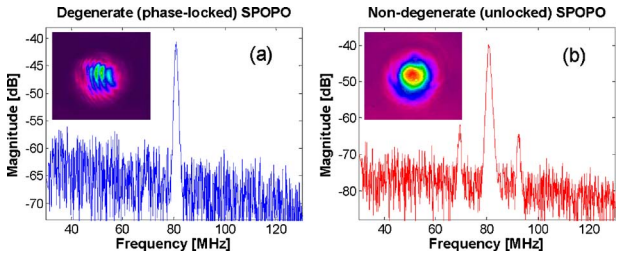


Fig. 9. (Color online) Results from interference between the pump and the OPO SH using a 1600 nm filter before the SH crystal for (a) degenerate (phase-locked) and (b) non-degenerate (unlocked) SPOPOs. The data are consistent with those in Fig. 8.

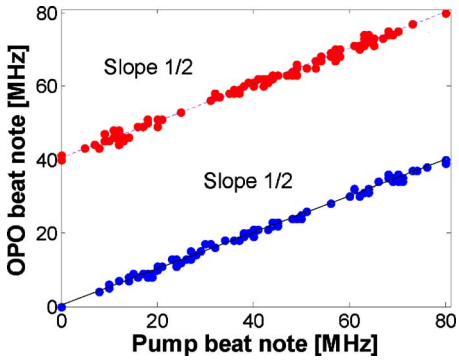


Fig. 10. (Color online) Scatter plot of beat notes between the phase-locked SPOPO and a CW laser at 1550 nm versus beat notes between the pump and frequency-doubled CW laser (at 775 nm). The slopes for the two sets of beat notes are both one half.

represents the locking range $\Delta f$ measured as a function of times above threshold for two different outcoupler (OC) mirrors of 50% and 25%, where one can see that the locking range monotonically increases with the pump power. The lines represent predictions of our theoretical model (15). Clearly, there is a very good match between experiment and theory. For the same number of times above threshold, the 50% output coupling yielded a broader detuning range compared to the 25% output coupler, again in agreement with theory.

The average output power of the degenerate SPOPO with the 50% OC mirror was 250 mW at 900 mW of the average pump power. The pump threshold was 140 mW, the slope efficiency was 32%, and the pump depletion exceeded 60%. For the 25% OC, the pump threshold was 35 mW.

The mode-locked pump laser was free-running (no CEO stabilization applied) and no feedback servo loop was needed for the SPOPO to maintain oscillation (the only measures we used against environmental noise were a floated optical table and an enclosure built around the SPOPO). Despite the lack of active stabilization, the phase-locked operation of the SPOPO persisted even in the presence of intentional perturbations (e.g., tapping on the enclosure). Our understanding of the physical mechanism for the phase-locked operation is that it is more advantageous for the signal and the idler modes to follow exactly the same frequency grid, because in this case a larger parametric gain is achieved. Since the signal and

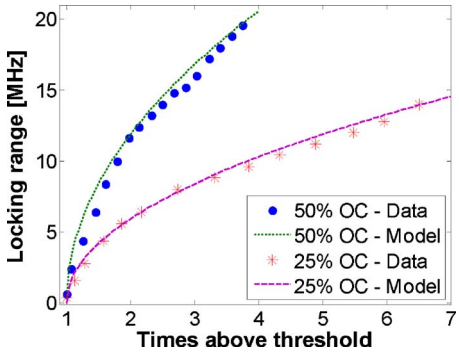


Fig. 11. (Color online) Measured data and calculated curves of the frequency locking range $\Delta f$ as a function of number of times above pump threshold for the 50% and 25% output coupling.

the idler become indistinguishable, deterministic phase relation between the pump and the OPO modes is established through Eq. (7).

## 5. CONCLUSION

In the past, types I and 0 degenerate mode-locked OPOs have been avoided due to the common misperception that such systems are inherently unstable and impractical, thus requiring exceptional control to operate. We show that the SPOPO is inherently stable when it runs in the degenerate self-phase-locked regime. Future directions for this work include exploring new spectral ranges and broadening the bandwidth of the frequency comb to at least an octave. The latter can be achieved by extending the phase-matching gain bandwidth by using shorter nonlinear crystals and also by precise cavity dispersion control using chirped dielectric mirrors.

## ACKNOWLEDGMENTS

We would like to thank Tomas Plettner for helpful discussions, and Karel Urbanek and Carsten Langrock for experimental support.

## REFERENCES

1. T. Udem, R. Holzwarth, and T. W. Hänsch, "Optical frequency metrology," Nature **416**, 233–237 (2002).
2. S. T. Cundiff and J. Ye, "Colloquium: femtosecond optical frequency combs," Rev. Mod. Phys. **75**, 325–342 (2003).
3. T. Steinmetz, T. Wilken, C. Araujo-Hauck, R. Holzwarth, T. W. Hänsch, L. Pasquini, A. Manescau, S. D'Odorico, M. T. Murphy, T. Kentischer, W. Schmidt, and T. Udem, "Laser frequency combs for astronomical observations," Science **321**, 1335–1337 (2008).
4. M. J. Thorpe, D. Balslev-Clausen, M. S. Kirchner, and J. Ye, "Cavity-enhanced optical frequency comb spectroscopy: Application to human breath analysis," Opt. Express **16**, 2387–2397 (2008).
5. F. Keilmann, C. Gohle, and R. Holzwarth, "Time-domain mid-infrared frequency-comb spectrometer," Opt. Lett. **29**, 1542–1544 (2004).
6. E. Sorokin, I. T. Sorokina, J. Mandon, G. Guelachvili, and N. Picqué, "Sensitive multiplex spectroscopy in the molecular fingerprint 2.4 $\mu$m region with a $Cr^{2+}$:ZnSe femtosecond laser," Opt. Express **15**, 16540–16545 (2007).
7. J. Mandon, G. Guelachvili, and N. Picque, "Fourier transform spectroscopy with a laser frequency comb," Nat. Photonics **3**, 99–102 (2009).
8. M. Hentschel, R. Kienberger, C. Spielmann, G. A. Reider, N. Milosevic, T. Brabec, P. Corkum, U. Heinzmann, M. Drescher, and F. Krausz, "Attosecond metrology," Nature **414**, 509–513 (2001).
9. P. B. Corkum and F. Krausz, "Attosecond science," Nat. Phys. **3**, 381–387 (2007).
10. T. Plettner, R. L. Byer, E. Colby, B. Cowan, C. M. S. Sears, J. E. Spencer, and R. H. Siemann, "Visible-laser acceleration of relativistic electrons in a semi-infinite vacuum," Phys. Rev. Lett. **95**, 134801 (2005).
11. C. M. S. Sears, E. Colby, R. J. England, R. Ischebeck, C. McGuinness, J. Nelson, R. Noble, R. H. Siemann, J. Spencer, D. Walz, T. Plettner, and R. L. Byer, "Phase stable net acceleration of electrons from a two-stage optical accelerator," Phys. Rev. Lett. **11**, 101301 (2008).
12. B. M. Cowan, "Three-dimensional dielectric photonic crystal structures for laser-driven acceleration," Phys. Rev. ST Accel. Beams **11**, 011301 (2008).
13. I. S. Moskalev, V. V. Fedorov, and S. B. Mirov, "Self-starting Kerr-mode-locked polycrystalline $Cr^{2+}$:ZnSe laser," in *The CLEO/QELS Conference* (Optical Society of America, 2008), paper CF13.
14. C. L. Hagen, J. W. Walewski, and S. T. Sanders, "Generation of a continuum extending to the midinfrared by pumping ZBLAN fiber with an ultrafast 1550-nm source," IEEE Photon. Technol. Lett. **18**, 91–93 (2006).
15. C. Xia, M. Kumar, O. P. Kulkarni, M. N. Islam, F. L. Terry, M. J. Freeman, M. Poulain, and G. Mazé, "Midinfrared supercontinuum generation to 4.5 $\mu$m in ZBLAN fluoride fibers by nanosecond diode pumping," Opt. Lett. **31**, 2553–2555 (2006).
16. J. Mandon, E. Sorokin, I. T. Sorokina, G. Guelachvili, and N. Picqué, "Supercontinua for high-resolution absorption multiplex infrared spectroscopy," Opt. Lett. **33**, 285–287 (2008).
17. C. Langrock, M. M. Fejer, I. Hartl, and M. E. Fermann, "Generation of octave-spanning spectra inside reverse-proton-exchanged periodically poled lithium niobate waveguides," Opt. Lett. **32**, 2478–2480 (2007).
18. A. Bonvalet, M. Joffre, J. L. Martin, and A. Migus, "Generation of ultrabroadband femtosecond pulses in the mid-infrared by optical rectification of 15 fs light pulses at 100 MHz repetition rate," Appl. Phys. Lett. **67**, 2907–2909 (1995).
19. R. A. Kaindl, M. Wurm, K. Reimann, P. Hamm, A. M. Weiner, and M. Woerner, "Generation, shaping, and characterization of intense femtosecond pulses tunable from 3 to 20 $\mu$m ," J. Opt. Soc. Am. B **17**, 2086–2094 (2000).
20. S. M. Foreman, D. J. Jones, and J. Ye, "Flexible and rapidly configurable femtosecond pulse generation in the mid-IR," Opt. Lett. **28**, 370–372 (2003).
21. C. Erny, K. Moutzouris, J. Biegert, D. Kühlke, F. Adler, A. Leitenstorfer, and U. Keller, "Mid-infrared difference-frequency generation of ultrashort pulses tunable between 3.2 and 4.8 $\mu$m from a compact fiber source," Opt. Lett. **32**, 1138–1140 (2007).
22. A. Gambetta, R. Ramponi, and M. Marangoni, "Mid-infrared optical combs from a compact amplified Er-doped fiber oscillator," Opt. Lett. **33**, 2671–2673 (2008).
23. P. Malara, P. Maddaloni, G. Gagliardi, and P. De Natale, "Absolute frequency measurement of molecular transitions by a direct link to a comb generated around 3-$\mu$m ," Opt. Express **16**, 8242–8249 (2008).
24. J. H. Sun, B. J. S. Gale, and D. T. Reid, "Composite frequency comb spanning 0.4–2.4 $\mu$m from a phase-controlled femtosecond Ti:sapphire laser and synchronously pumped optical parametric oscillator," Opt. Lett. **32**, 1414–1416 (2007).
25. F. Adler, K. C. Cossel, M. J. Thorpe, I. Hartl, M. E. Fermann, and J. Ye, "Phase-stabilized, 1.5 W frequency comb at 2.8–4.8 $\mu$m ," Opt. Lett. **34**, 1330–1332 (2009).
26. D. Brida, C. Manzoni, G. Cirmi, M. Marangoni, S. De Silvestri, and G. Cerullo, "Generation of broadband mid-infrared pulses from an optical parametric amplifier," Opt. Express **15**, 15035–15040 (2007).
27. C. D. Nabors, S. T. Yang, T. Day, and R. L. Byer, "Coherence properties of a doubly-resonant monolithic optical parametric oscillator," J. Opt. Soc. Am. B **7**, 815–820 (1990).
28. N. C. Wong, "Optical frequency division using an optical parametric oscillator," Opt. Lett. **15**, 1129–1131 (1990).
29. E. J. Mason and N. C. Wong, "Observation of two distinct phase states in a self-phase-locked type II phase-matched optical parametric oscillator," Opt. Lett. **23**, 1733–1735 (1998).
30. C. Fabre, E. J. Mason, and N. C. Wong, "Theoretical analysis of self-phase-locking in a type II phase-matched optical parametric oscillator," Opt. Commun. **170**, 299–307 (1999).
31. P. Gro$\beta$ and K. J. Boller, "Stability analysis of the self-phase-locked divide-by-2 optical parametric oscillator," Phys. Rev. A **71**, 033801 (2005).
32. P. Gro$\beta$, K. J. Boller, and M. E. Klein, "High-precision wavelength-flexible frequency division for metrology," Phys. Rev. A **71**, 043824 (2005).
33. G. Kalmani, A. Arie, P. Blau, S. Pearl, and A. V. Smith,

"Polarization-mixing optical parametric oscillator," Opt. Lett. **30**, 2146–2148 (2005).
34. D. H. Lee, M. E. Klein, J. P. Meyn, P. Gro$\beta$, R. Wallenstein, and K. J. Boller, "Self-injection-locking of a CW-OPO by intracavity frequency-doubling the idler wave," Opt. Express **5**, 114–119 (1999).
35. J. Zondy, A. Douillet, A. Tallet, E. Ressayre, and M. Le Berre, "Theory of self-phase-locked optical parametric oscillator," Phys. Rev. A **63**, 023814 (2001).
36. D. H. Lee, M. E. Klein, J. P. Meyn, R. Wallenstein, P. Gro$\beta$, and K. J. Boller, "Phase-coherent all-optical frequency division by three," Phys. Rev. A **67**, 013808 (2003).
37. Y. Kobayashi and K. Torizuka, "Measurement of the optical phase relation among sub-harmonic pulses in a femtosecond optical parametric oscillator," Opt. Lett. **25**, 856–858 (2000).
38. Y. Kobayashi and K. Torizuka, "Carrier-phase control among subharmonic pulses in a femtosecond optical parametric oscillator," Opt. Lett. **26**, 1295–1297 (2001).
39. Y. Kobayashi, H. Takada, M. Kakehata, and K. Torizuka, "Optical phase locking among subharmonic pulses," Opt. Lett. **28**, 1377–1379 (2003).
40. S. T. Wong, T. Plettner, K. L. Vodopyanov, K. Urbanek, M. Digonnet, and R. L. Byer, "Self-phase-locked degenerate femtosecond optical parametric oscillator," Opt. Lett. **33**, 1896–1898 (2008).
41. S. T. Wong, "Self-phase-locking of degenerate synchronously pumped optical parametric oscillators," Ph.D. dissertation (Stanford University, 2009).
42. J. A. Armstrong, N. Bloembergen, J. Ducuing, and P. S. Pershan, "Interactions between light waves in a nonlinear dielectric," Phys. Rev. **127**, 1918–1939 (1962).
43. A. Yariv, *Quantum Electronics*, 3rd ed. (Wiley, 1998), pp. 412–416.